The Tokyo Axion Helioscope

```
R. Ohta<sup>a,*</sup>, Y. Akimoto<sup>b</sup>, Y. Inoue<sup>c,h</sup>, M. Minowa<sup>a,h</sup>, T. Mizumoto<sup>d</sup>, S.
                     Moriyama<sup>e</sup>, T. Namba<sup>c</sup>, Y. Takasu<sup>f</sup>, A. Yamamoto<sup>g,h</sup>
     <sup>a</sup>Department of Physics, School of Science, University of Tokyo, 7-3-1 Hongo, Bunkyo-ku,
                                           Tokyo 113-0033, Japan
     <sup>b</sup>School of Science, University of Tokyo, 7-3-1 Hongo, Bunkyo-ku, Tokyo 113-0033, Japan
     <sup>c</sup>International Center for Elementary Particle Physics, University of Tokyo, 7-3-1 Hongo,
                                    Bunkyo-ku, Tokyo 113-0033, Japan
                <sup>d</sup>Department of Physics, Graduate School of Sciene, Kyoto University,
                      Kitashirakawa-oiwake-cho, Sakyo-ku, Kyoto 606-8502, Japan
           <sup>e</sup>Institute for Cosmic Ray Research, University of Tokyo, 456 Higashi-Mozumi,
11
                                Kamioka-cho, Hida, Gifu 506-1205, Japan
12
                                          <sup>f</sup>Tsukuba, Ibaraki, Japan
13
       <sup>9</sup>High Energy Accelerator Research Organization, 1-1 Oho, Tsukuba, Ibaraki 305-0801,
14
15
                                                     Japan
       <sup>h</sup>Research Center for the Early Universe (RESCEU), School of Science, University of
16
                        Tokyo, 7-3-1 Hongo, Bunkyo-ku, Tokyo 113-0033, Japan
17
```

Abstract

The Tokyo Axion Helioscope experiment aims to detect axions which are produced in the solar core. The helioscope uses a strong magnetic field in order to convert axions into X-ray photons and has a mounting to follow the sun very accurately. The photons are detected by an X-ray detector which is made of 16 PIN-photodiodes. In addition, a gas container and a gas regulation system is adopted for recovering the coherence between axions and photons in the conversion region giving sensitivity to axions with masses up to 2 eV. In this paper, we report on the technical detail of the Tokyo Axion Helioscope.

19 Keywords: solar axion, helioscope, PIN photodiode, superconducting magnet

1. Introduction

- Axions are light neutral pseudoscalar particles which are introduced to solve
- the strong CP problem [1]. They would be produced in the solar core via the
- ²³ Primakoff conversion of the plasma photons if they have large enough coupling
- to photons [2] [3]. The Tokyo Axion Helioscope experiment (also known as

^{*}Corresponding author.

Sumico experiment) aims to detect solar axions by tracking the sun (Fig. 1).

The helioscope consists of a tracking system, a superconducting magnet, a gas



Figure 1: Photograph of Tokyo Axion Helioscope

6

regulation system, and an X-ray detector. The magnet, the gas container and the X-ray detector are assembled in a 3-m long cylinder. The tracking system supports and drives the cylinder of the helioscope to align the helioscope axis with the direction of the sun.

Axions are converted into photons with energy of several keV, reflecting temperature of the solar core. These photons are detected by an X-ray detector. The detection principle is based on the coupling of an incoming axion to a virtual photon provided by the transverse magnetic field of an intense dipole magnet. Thus the incoming axion is converted into a real, detectable photon that carries the energy of the original axion. The conversion rate is given by [3]

$$P_{a \to \gamma} = \left| \frac{g_{a\gamma\gamma}}{2} \exp\left[-\int_0^L dz \ \Gamma/2 \right] \times \int_0^L dz B_\perp \exp\left[i \int_0^z dz' \left(q - \frac{i\Gamma}{2} \right) \right] \right|^2, \quad (1)$$

where $g_{a\gamma\gamma}$ is the coupling constant between axions and photons, z and z' are

the coordinate along the incoming axion, B_{\perp} is the strength of the transverse magnetic field, L is the length of the field along z-axis, Γ is the X-ray absorption 33 coefficient of medium with which the conversion region is filled, $q=(m_{\gamma}^2$ $m_a^2/2E$ is the momentum transfer by the virtual photon, and m_{γ} is the effective mass of the photon which equals to zero in vacuum. Axions have not been discovered yet in any of the past experiments. In 37 the first phase [4] of our experiment, the conversion region was vacuum and the experimental limit is given to be $g_{a\gamma\gamma} < 6.0 \times 10^{-10} \, \mathrm{GeV^{-1}}$ (95% C.L.) for $m_a < 0.03\,\mathrm{eV}$. To detect heavy axions, the momentum transfer should be kept negligible by introducing a dispersion matching medium into the conversion region. For this purpose, helium gas was used in the second phase [5] and the 42 limit is given to be $g_{a\gamma\gamma} < 6.3 - 10.5 \times 10^{-10} \,\mathrm{GeV^{-1}}$ (95% C.L.) for $m_a < 0.27 \,\mathrm{eV}$. The third phase [6] was also performed using denser helium gas than that of the

In this paper, we report on the technical detail of the Tokyo Axion Helio-scope.

second one and the limit is given to be $g_{a\gamma\gamma} < 5.6 - 13.4 \times 10^{-10} \, \mathrm{GeV^{-1}}$ (95%)

⁴⁹ 2. Tracking System

C.L.) for $0.84 < m_a < 1.00 \,\text{eV}$.

The tracking system consists of a driving mechanism, direction measuring encoders and a PC (computer 1). They form a feedback control loop as a whole.

A schematic view of the driving system is shown in Fig. 2. We adopted an altazimuth mount as the driving mechanism. The altazimuth mount minimizes inclination of the refrigerator and can support the magnet with simple structure.

The driving mechanism is composed of an axle bearing, a turntable, a ball screw, and two AC servomotors. The cylinder is supported by the axle bearing on the turntable. In the azimuthal direction, the turntable is driven by one of the servomotors (Hitachi EPS8). In the altitudinal direction, the cylinder is driven by the other servomotor (Hitachi EPL3TD) through the ball screw.

The axion helioscope is located in Tokyo at 139°45′48"E and 35°42′49"N.

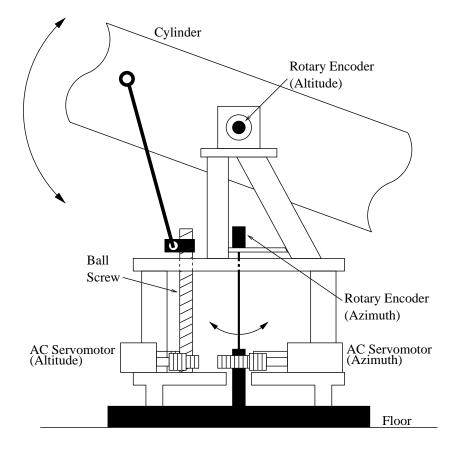


Figure 2: Schematic view of driving system

- In usual operation, the driving range of the helioscope is from -28° to 28° in
- the altitudinal direction and the range of the azimuthal direction is 360°. Its
- azimuthal direction is limited only by a limiter which prevents the helioscope
- from endless rotation. Within this limitations, the helioscope can track the Sun
- 65 half of a day averagely.
- The control diagram of the tracking system is shown in Fig. 3. The driving
- 67 mechanism is wholly controlled by computer 1 via CAMAC bus.
- The azimuthal and altitudinal directions of the helioscope are measured by
- 69 two precision rotary encoders (Canon R-1 L) each of which produces 81,000
- pulse-per-revolution quadrature outputs in A and B channels and a zero index

output in Z channel to indicate its angular origin. The encoder pulses are sent to a homemade pulse counter by which computer 1 obtains the absolute angle of each encoders with a resolution of 1/324,000 revolution or 4 arcseconds (ca. $19 \,\mu\text{rad}$).

Each AC servomotor is controlled through a homemade CAMAC pulse generator. Every 0.2 second, computer 1 calculates the amount and the frequency of the pulses, namely the angle and the speed of rotation, for the next period based on the measured- and targeted directions of the helioscope.

The overall tracking accuracy is better than 0.5 mrad both in altitudinal and

azimuthal direction. Main components of the errors are the fluctuation of the turntable and the misalignment of the magnet aperture and the helioscope axis.

The guidance of the helioscope movement is provided by the tracking software. In order to calculate the position of the sun, the U. S. Naval Observatory Vector Astronomy Subroutines (NOVAS-C ver 2.0.1) [7] is used. NOVAS-C calculates the topocentric position of the sun with less than 2 arcseconds (= $9.7 \mu rad$) error which is negligible in our measurements.

87 3. Superconducting Magnet

79

Incoming solar axions are converted into photons by magnetic field of the superconducting magnet. The conversion efficiency of axions depends strongly on the strength and length of the magnetic field as shown in Eq.(1).

Two devices make it easy to swing the magnet. Firstly, the magnet is made cryogen-free by using two Gifford-McMahon refrigerators (GM refrigerators).

Therefore, no liquid helium tube is needed. Secondly, a persistent current switch (PCS) is equipped and the magnet is free from thick current leads.

95 3.1. Magnet and Cryogenics

The superconducting magnet consists of two 2.3-m long race-track shaped coils running parallel with a 20-mm wide gap between them. In this gap, the gas container is inserted and axions are converted into photons, which are to

be detected by the X-ray detector. A schematic view of the magnet is shown in Fig. 4. 100

The coils are made of copper-clad NbTi superconducting wires and housed in a stainless steel case. They are kept at 5-6 K during operation. The magnetic 102 field in the gap is about 4 T perpendicular to the helioscope axis when a current 103 is 268 A. The magnet is cooled by two GM refrigerators each of which is two 104 staged. The radiation shield of the cryostat is connected with the first-stage cold 105 heads where the temperature reaches about 40 K in normal operation. The coils are connected with the second stage, which reaches about 4K, through a ther-107 mal conductive rod and plates made of oxygen-free high-conductivity (OFHC) 108 copper. High- T_c superconducting current leads are used between the first and 109 the second stages. 110

Thermometers are attached to the coils, cold heads of refregerators etc. to 111 measure the temperature distribution. As thermometers, Carbon Glass Resis-112 tors (CGRs) and platinum-cobalt resistors (PtCos) are used. CGRs are used to 113 measure low temperatures (5–10 K) and PtCos are sensitive at relatively high 114 temperatures (10–300 K). Each CGR was calibrated by the manufacturer. Two Hall sensors are also attached to the coils to measure the strength of the mag-116 netic field. 117

3.2. Persistent Current Switch

127

The magnet can be operated in persistent current mode by short-circuiting the coils with the persistent current switch (PCS) [8]. In Fig. 5, a circuit 120 diagram of the magnet is shown. In this mode, the power supply is no longer 121 needed to maintain the magnetic field and the current leads can be disconnected 122 completely. 123

The PCS is mounted on a copper plate which is weakly coupled to the second stage of the refrigerators. The PCS is made of superconducting wire and 125 an integrated heater to change its phase to normal phase. Before exciting the 126 magnet, the heater is switched on and keeps the temperature of the PCS above 9 K, which is the phase-transition temperature of the wire used in the PCS. The PCS in normal phase has resistance around $11\,\Omega$. Then a magnet excitation starts with supplying current. When the current reaches the final value, excitation voltage goes to zero and the heater is switched off to cool the PCS down.

After the PCS goes back to superconducting phase, the supplying current can be decreased to zero while the current in the main circuit is maintained.

4. Gas Regulation System

135

4.1. Coherence between Axion and Photon

To keep coherence between axion and photon, m_{γ} has to be tuned to m_a by introducing gas into the conversion region. For this purpose, the gas container is inserted into the aperture of the magnet.

A photon in the X-ray region acquires a positive effective mass in a medium. It is well approximated by

 $m_{\gamma} = \sqrt{\frac{4\pi\alpha N_e}{m_e}} \tag{2}$

as for the light gas, such as hydrogen or helium, where α is the fine structure 139 constant, m_e is the electron mass, and N_e is the number density of electrons [3]. Cold helium gas was adopted as a dispersion matching medium, because helium 141 gas has small X-ray absorption length and remains at gas state at 5 K, the 142 operating temperature of our magnet, at 1 atm. If m_a differs from m_{γ} , coherence 143 between axion and photon is lost and the conversion efficiency decreases. From 144 Eq. (1), the condition in which the conversion efficiency has significant value is $qL \lesssim \pi$. For a given effective mass, axion masses m_a within a very narrow range satisfy this condition. The width of this window is about 2 meV (FWHM) at 147 $m_{\gamma} \simeq 1 \, \text{eV}$. To sweep the axion mass range up to a few eV, we need to change 148 the gas density more than a thousand times. To control the gas density, we 149 need to control the pressure accurately and to keep the temperature constant. Therefore we developed an automatic pressure and temperature control system 151 of helium gas in the gas container for the third phase of solar axion search [6].

4.2. Gas Container

153

The body of the container is made of four 2.3-m long 0.8-mm thick stainless-154 steel rectangle pipes welded side by side to each other. The entire body is 155 wrapped with 5N high purity aluminum sheet to achieve high uniformity of temperature. The measured thermal conductance between the both ends was 157 $1 \times 10^{-2} \,\mathrm{W/K}$ at 6 K when the magnetic field is 4 T. One end at the forward 158 side of the container is sealed with welded plugs and is suspended firmly by 159 three Kevlar cords, so that thermal flow through this end is highly suppressed. The opposite side nearer to the X-ray detectors is flanged and fixed to the 161 magnet. At this end of the container, gas is separated from vacuum with an 162 X-ray window (Fig. 6) manufactured by METOREX which is transparent to X-163 ray above 2 keV and can hold gas up to 0.3 MPa at liquid helium temperature. 164 The window is composed of 25- μ m thick Be foils, 1.5- μ m Ni support grids and Ni frames. The foils have 1- μ m polyimide coat on the one side. Though He gas at 6 K and 0.3 MPa corresponds to the effective mass of about 4 eV, absorption 167 of the gas becomes dominant and sensitivity of the apparatus decreases in this 168 mass region. 169

170 4.3. Pressure Control System

To change effective mass of photon in the gas container, we developed the 171 pressure control system of which diagram is shown in Fig. 7. Main compo-172 nents of this system are the gas container, a precision pressure gauge (YOKO-173 GAWA MU101-AH1N), a helium gas bottle for providing gas, a diaphragm pump (Pfeiffer Vacuum MVP 015-4) for suction, PCs for automatic regulation, 175 and three piezo-valves (HORIBA STEC PV-1000 series). The helium gas is 176 injected through PV1 and is sucked by the vacuum pump through PV2 or PV3. 177 The gas pressure is regulated by changing the gas flows through the piezo-valves 178 which are controlled by their control voltages. Two PV-1101 piezo-valves are used in PV1 and PV2, while a PV-1302 is used in PV3. PV3 is used to reach 180 lower pressures below 10 kPa, where the suction is not enough only with PV2. 181

The gas flow of a PV-1302 is 30 times as high as a PV-1101. Control voltages are supplied by computer 2 through a digital to analog converter (Interface PCI-3521).

In the third phase of this experiment, mass scanning was performed changing the effective mass by decreasing the pressure step by step. In fact, PV1 was opened only at the early stages of the scan until the gas pressure reached the highest value p_s^{\max} , and was closed during the automatic-control sequences. The automated sequences worked as follows:

- While the measured pressure p_m was higher than the set pressure of a period p_s , PV2 (or PV3) was opened proportionally to $\Delta p = p_m p_s$ as far as the flow rate was within the capability of the value. For larger Δp , PV2 (or PV3) was fully opened. The coefficient was determined empirically.
- Once p_m became less than p_s , PV2 (or PV3) was closed and remained closed during measurement.
 - When a measurement had finished, p_s was set to the next value and a new sequence was repeated.

199 4.4. Temperature Control System

190

191

192

193

194

197

198

Because the gas container is fixed on the magnet which is thermally coupled to the GM refrigerators, the temperature of the gas container is affected by fluctuations of the cooling power of the refrigerators. We developed a temperature control system, since it is crucial to keep the gas temperature constant to retain density uniformity of the gas as well as to control its density reliably.

The diagram of the temperature control system is shown in Fig. 8. The main components of this system are a heater and a CGR thermometer T5. T5 is measuring the temperature of a copper plate which is tightly joined with the gas container. The heater is attached to the heat link between the copper plate and the magnet. The current through the heater is controlled to keep the T5

temperature constant, where PI (Proportional-Integral) control is adopted. The
PI parameters are decided empirically.

5. X-ray detector

213 5.1. PIN Photodiode X-ray Detector

The X-ray detector to detect photons originating from axions consists of 16
PIN photodiodes, Hamamatsu Photonics S3590-06-SPL(Fig. 9), and 16 preamplifiers which amplify signals from the PIN photodiodes.

Each of preamplifiers is separated into two part called head and back-end part. The head parts are mounted next to the photodiodes and include the first stage FETs, feedback resistors, test pulse inputs and HV buffers. The PIN photodiodes and the head parts are assembled in the helioscope cylinder. The remaining circuits are placed out of the cylinder. The details of this X-ray detector is described elsewhere [9] [10].

223 5.2. Data Acquisition System

The output signals of the preamplifiers are stored and analyzed so that we will obtain energy spectrum of the signals. The data acquisition system is shown in Fig. 10.

Firstly, signals from preamplifiers are filtered and low frequency components are reduced. Since the cut off frequency of this filter is 3 kHz, it does not affect X-ray signals whose rise time is $0.8-1.3\,\mu$ s but reduce microphonic noise. Next, the filtered signal is amplified by a linear amplifier called the booster with a gain of about 300 to fit the input range of the FADCs. These filter and booster are mounted just beside the back-end parts of the preamplifiers.

After the booster, signals are sent to the FADCs (REPIC RPC-081) via 15m coaxial cables. The sampling period of the FADC is $0.1 \,\mu\text{s}$, the resolution is 8 bit, and the buffer depth is 1024 words. The FADCs are stopped $50 \,\mu\text{s}$ after the trigger signal is latched in the input registers (HOSHIN C005). The trigger is made from a discriminator (Technoland N-TM405) and a shaping amplifier (Clear-Pulse 4026) whose shaping time is $3 \mu s$. When the FADC is stopped by trigger, the input register tell the trigger to computer 1 and it takes waveform from the FADCs via CAMAC bus. At the same time the livetime counter is stopped. Because deadtime of each transfer is about 0.35s and cannot be ignored in the measurement, the livetime is counted in millisecond accuracy by a 1-kHz clock. This accuracy is needed to compare the solar tracking event and the non-tracking event.

245 6. Summary

We developed the axion helioscope which aims to detect solar axions. This 246 experimental apparatus consists of the tracking system, the superconducting 247 magnet, the gas regulation system, and the X-ray detector. The tracking sys-248 tem directs the main cylinder towards the sun. The magnet converts incoming 249 axions into photons and the unmanned gas regulation system enables us to 250 convert axions with masses up to eV scale. The X-ray detector measures conversion photons and the DAQ system records the signal of the photons into the 252 computer. Using this apparatus, we have performed solar axion searches with 253 axion's mass up to 0.27 eV [4] [5] and around 1 eV [6]. Since we did not detect 254 an evident signal of axion, we are going to perform more massive solar axion search with mass up to about 2 eV in the near future. 256

7. Acknowledgements

The authors thank the former director general of KEK, Professor H. Sugawara, for his support in the beginning of the helioscope experiment. This research was partially supported by Grant-in-Aid for COE Research, the Japanese
Ministry of Education, Science, Sports and Culture (MEXT) and Grant-in-Aid
for Scientific Research (B), Japan Society for the Promotion of Science and also
by the Matsuo Foundation. Additional support was provided by Global COE
Program "Physical Sciences Frontier", MEXT, Japan.

265 References

- [1] R. D. Peccei, H. R. Quinn, Phys. Rev. Lett. 38 (1977) 1440; R. D. Peccei,
 H. R. Quinn, Phys. Rev. D 16 (1977) 1791.
- ²⁶⁸ [2] P. Sikivie, Phys. Rev. Lett. 51 (1983) 1415.
- [3] K. van Bibber, P. M. McIntyre, D. E. Morris, G. G. Raffelt, Phys. Rev. D
 39 (1989) 2089.
- [4] S. Moriyama, M. Minowa, Y. Inoue, T. Namba, Y. Takasu, A. Yamamoto,
 Phys. Lett. B 434 (1998) 147.
- [5] Y. Inoue, T. Namba, S. Moriyama, M. Minowa, Y. Takasu, T. Horiuch, A.
 Yamamoto, Phys. Lett. B 536 (2002) 18.
- [6] Y. Inoue, Y. Akimoto, R. Ohta, T. Mizumoto, A. Yamamoto, M. Minowa,
 Phys. Lett. B 668 (2008) 93.
- ²⁷⁷ [7] G. H. Kaplan, et al., Astronomical Journal 97 (1989) 1197.
- [8] S. Mizumaki, Ph. D thesis, "Study of the property of current propagation about superconductive junction", The Graduate University for Advanced Studies, Mar. 1997.
- [9] T. Namba, Y. Inoue, S. Moriyama, M. Minowa, Nucl. Instr. and Meth. A
 489 (2002) 224.
- [10] Y. Akimoto, Y. Inoue, M. Minowa, Nucl. Instr. and Meth. A 557 (2006)
 684.

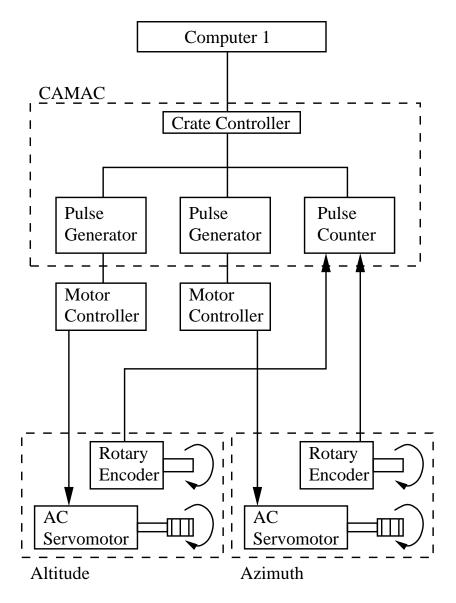


Figure 3: Control diagram of tracking system

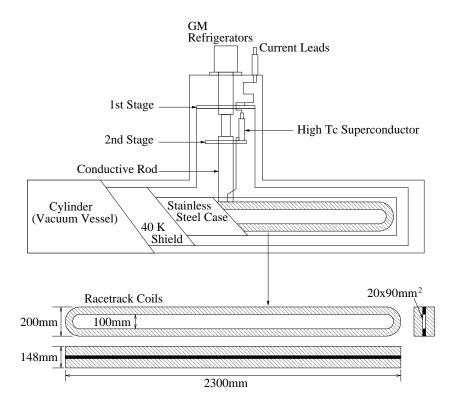


Figure 4: Schematic shape of race-track coils

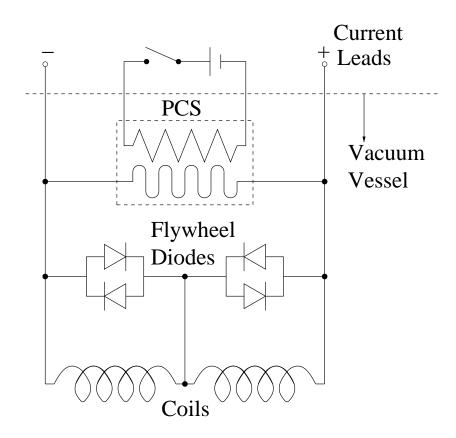


Figure 5: Circuit diagram of the magnet

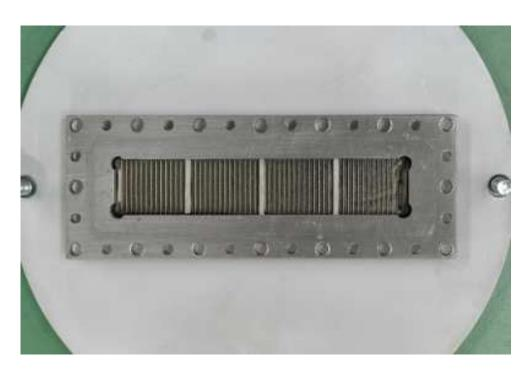


Figure 6: X-ray window

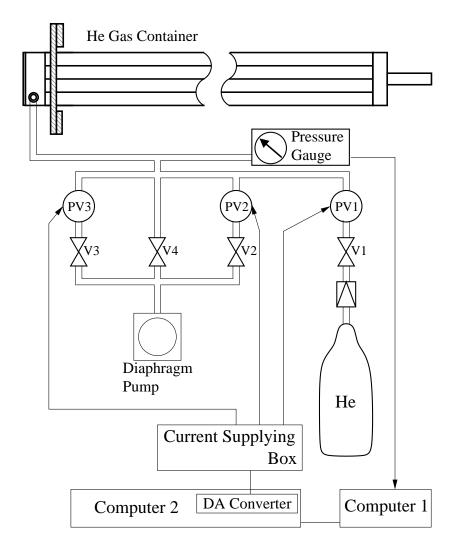


Figure 7: Diagram of pressure control system

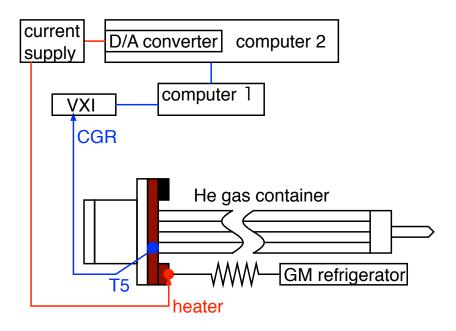


Figure 8: Diagram of temperature control system

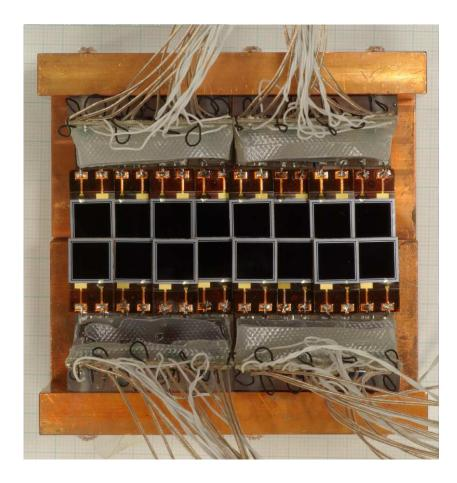


Figure 9: Photograph of PIN photodiode array

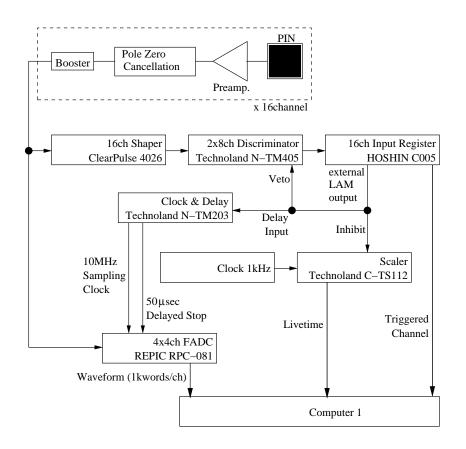


Figure 10: Diagram of DAQ system